Optical properties of TAl compounds (T=Fe, Co, Ni) and CoGa: role of the 3d semi-core states of Ga

1990 J. Phys.: Condens. Matter 2 465

(http://iopscience.iop.org/0953-8984/2/2/021)

J. Phys.: Condens. Matter 2 (1990) 465–478. Printed in the UK

Optical properties of TAl compounds (T = Fe, Co, Ni) and CoGa: role of the 3d semi-core states of Ga

D Knab and C Koenig
Institut de Physique et Chimie des Matériaux, Université Louis Pasteur, 4 rue Blaise Pascal, 67070 Strasbourg Cedex, France

Received 3 March 1989, in final form 11 September 1989

Abstract. In order to get a good overall description of the electronic structure of CoGa, it has been calculated self-consistently by the LMTO method, including the 3d semi-core states of Ga as lower band states participating in the charge transfer. Using self-consistent potentials derived previously for the series TAl (T = Fe, Co, Ni), the dielectric functions of all these compounds are calculated by a tetrahedron method taking properly into account the cut-off of the Fermi surface.

1. Introduction

The electronic structure of TAl compounds (T = V, Fe, Co, Ni) has been extensively studied by different techniques (Eibler and Neckel 1980, Whittle *et al* 1982, Koch and Koenig 1986) due to the great interest arising from the experimental study of magnetic impurities and intrinsic defects around the stoichiometry for these ordered compounds.

There is a good agreement between the different theoretical calculations concerning the density of states in these compounds: this density consists essentially of two 'd' peaks of symmetry t_{2g} and e_g, due to the transition atom, separated by a pseudogap. The Fermi level moves upwards from one peak to above the second peak when going through the series, in a nearly rigid-band way.

The contribution of one Ga atom to the conduction band of CoGa is two 's' electrons and one p electron, just as for Al in CoAl. Therefore, the two densities of states must be very similar as was found by Koch and Koenig (1986) using the 'linear muffin-tin orbitals method' (LMTO). But it was obvious in this latter work that the treatment of all the other Ga states as frozen core states is not well justified. The purpose of the present work is first to complete the studies already done on the band structure of CoGa by analysing the role of the semi-core 3d states. This will be discussed in the next section.

The self-consistent potentials we have obtained for the series TAl (Koch and Koenig 1986) and CoGa are a good starting point for the study of the optical properties of these compounds. The LMTO formalism is particularly well adapted to the calculation of the transition probabilities and has already been applied to different materials (Koenig and Khan 1983, Uspenski *et al* 1983, Maksimov *et al* 1988, Zemach *et al* 1989). For example, the calculated x-ray spectra obtained in LMTO by Alouani and Khan (1987) for FeAl compare as well with the experimental data as previous calculations performed using the augmented plane wave (APW) method by Schwartz *et al* (1979). Section 3 presents

0953-8984/90/020465 + 14 $03.50

Table 1. Core charge outside the WS spheres in CoAl, and in CoGa when 3d states of gallium are frozen ([Ar] $3d^{10}$) or unfrozen ([Ar]).

Site	Core charge to be renormalised (electrons)
Co	0.002
Al	0.001
Ga ([Ar]$3d^{10}$)	0.044
Ga ([Ar])	$<10^{-3}$

the calculated imaginary part of the dielectric function for the whole series of TAl compounds and CoGa, and compares it with other theoretical and experimental determinations of this function. Section 4 will be reserved for the conclusion.

2. Band structure of CoGa

The problem of semi-core states, which also exists in other compounds (Christensen and Kollar 1983, Norman and Koelling 1985, Koenig and Khan 1988), is linked to the validity of the frozen-core approximation often used in band structure calculations. The spin–orbit coupling being non-negligible in the inner shells, the core charge of each atom is obtained by solving the relativistic Dirac equation in the self-consistent atomic potential (Desclaux 1975). This core charge is then renormalised in the Wigner–Seitz (WS) sphere and kept frozen for the band structure calculation. It is obvious that this procedure gives correct results only if the core charge beyond the WS sphere is negligibly small. But in CoGa the 3d states of gallium are not very far from the bottom of the conduction band so that this condition is not fulfilled. The solution is, of course, to include the 3d levels in the band states. To perform this calculation, it is then necessary to introduce two energy panels, the first panel covering mainly the 3d states of gallium and the second the conduction band with gallium 4d states, with one set of potential parameters for each panel.

In this section we discuss the results obtained for CoGa within a one-panel or a two-panel calculation. In order to show the role of these 3d semi-core states in the conduction band, comparison is made with the electronic structure of CoAl, for which the frozen-core approximation is well justified. All these calculations are scalar relativistic. The Brillouin zone integrations for the densities of states are performed on a grid of 969 $\boldsymbol{k}$ points in the irreducible zone. The atomic radii are chosen to be equal to the WS radii for both components of the compounds. Other choices for these radii are possible (Koch and Koenig 1986, and references therein), which lead to very similar band structures. The departure from neutrality in each WS sphere, which is of course dependent of this choice, cannot be understood as an exact charge transfer from one atom to the other but gives nevertheless a good estimate of the electronic redistribution in the compound.

2.1. CoAl

In this compound the core charge barely extends beyond the WS sphere (R_{WS} = 2.663 au); the frozen-core approximation is good (table 1). The Fermi level is at 0.007

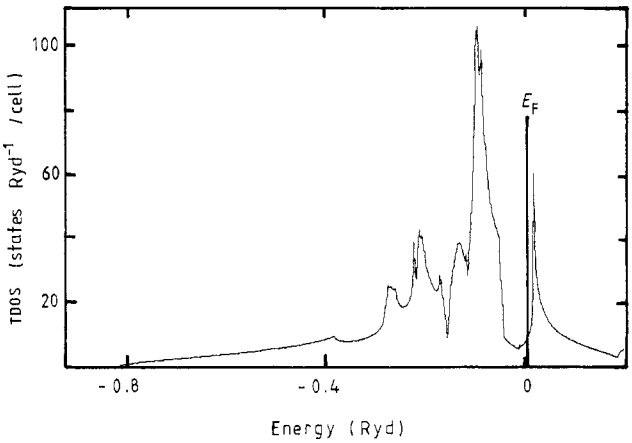

Figure 1. Total density of states in CoAl.

Table 2. Number of occupied states for s, p and d symmetries and total number of electrons at the two sites in CoAl, CoGa when 3d states of Ga are frozen and each panel of CoGa when 3d states are unfrozen. ΔQ is the departure from neutrality in each WS sphere.

	Co				Al/Ga				
	N_s	N_p	N_d	N_{tot}	N_s	N_p	N_0	N_{tot}	ΔQ
CoAl	0.624	0.832	7.906	9.362	0.884	1.315	0.439	2.638	0.362
CoGa (1 panel)	0.525	0.765	7.954	9.284	1.040	1.363	0.313	2.716	0.284
CoGa (2 panels)									
First panel	0.017	0.028	0.033	0.078	0.007	0.006	9.909	9.922	0.078
CoGa (2 panels)									
Second panel	0.562	0.757	7.905	9.224	1.071	1.394	0.311	2.776	0.224

Ryd in the pseudogap between the two d peaks of Co (figure 1). The numbers of states in each of the WS spheres for s, p and d symmetries show that there is essentially a transfer of s–p electrons of aluminium towards cobalt d states (table 2).

2.2. CoGa: one-panel calculation

The difference between CoGa and CoAl comes from the presence of 3d states in the gallium configuration which do not exist for Al. First these d states are included as core states. In this case, as for CoAl, the calculation is performed in one energy panel for the conduction band. The WS radii are taken equal to 2.681 au.

The density of states obtained for CoGa presents the same characteristics as the one obtained for CoAl. The Fermi level is also in the pseudogap, at 0.017 Ryd. The charge transfer, as in CoAl, is especially from gallium s–p states to cobalt d states (table 2). But, in this one-panel calculation, the gallium core charge ($[Ar]3d^{10}$) to renormalise within the WS sphere is larger than 0.04 electrons (table 1). The gallium 3d states are not very well localised and the frozen-core approximation is no longer good for these states.

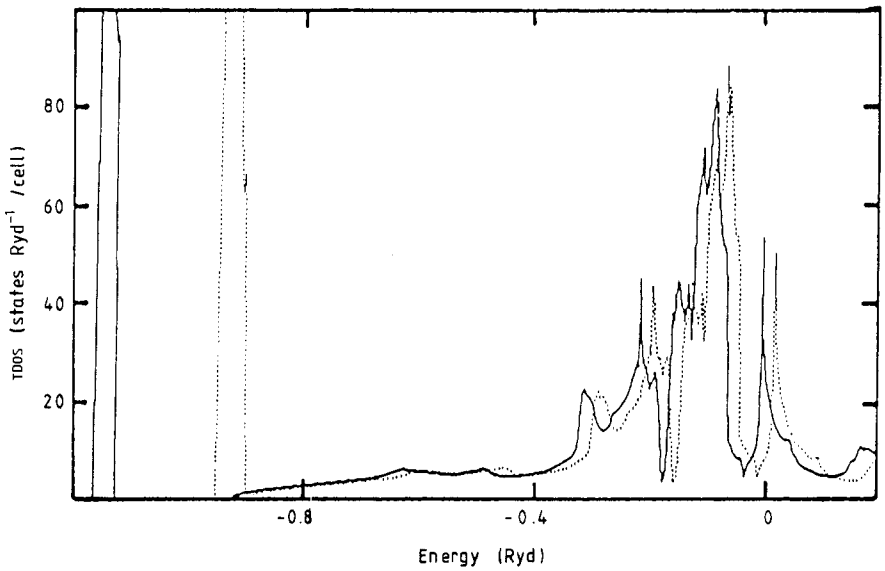

Figure 2. Total density of states in CoGa: dotted curves, when 3d orbitals of gallium are frozen; full curves, when they are unfrozen.

In order to estimate the errors arising from this renormalisation, it is interesting to recalculate the position of these 3d states when they are treated as band states in the self-consistent one-panel potential. They now form a narrow band which nearly touches the bottom of the conduction band, which is obviously an unphysical result (Koch and Koenig 1986, and figure 2). This shows that a one-panel calculation cannot provide a good description of the energy states around the bottom of the conduction band.

2.3. CoGa: two-panel calculation

The gallium 3d states are now treated self-consistently as band states hybridised with the conduction band. The remaining gallium core charge to renormalise ([Ar]) becomes negligible (table 1), so that the frozen-core approximation is good.

In this two-panel calculation, the density of states of the conduction band is almost unaffected by the modification of the treatment of the core charge, except for a slight global downwards shift of about 0.03 Ryd. This is not always the case. In $LaPd_3$, for example, where the 5p states of La play the same role as the 3d states of Ga in CoGa (Koenig and Khan 1988), the delocalisation of these states leads to a deformation of the conduction band by a lowering of the 4f peak with respect to the s, p and d states.

The self-consistent position of the band formed by the 3d states of gallium is now at about -1.14 Ryd, which means a shift of 0.22 Ryd towards lower energies compared with its position in the preceding case (figure 2). The two-panel calculation gives, therefore, a better description of the region beneath the conduction band. By forming a lower band in the compound, the 3d Ga states are even less localised on the Ga sites than the corresponding 3d core states in the isolated atoms: 0.08 electrons spread outside the WS sphere instead of 0.04. But the presence of this extra band forbids a part of the transfer of s–p electrons of gallium towards d states of cobalt in the conduction states

(about 0.06 electrons), so that the difference between the two-panel and the one-panel global charge transfer is only 0.02 electrons.

2.4. Discussion

The two principal effects on the density of states of CoGa of the inclusion of the 3d states of gallium in the self-consistent process are:

(i) a slight shift of the conduction band towards the lower energies with nearly no deformation,

(ii) the correction of the bad position in energy for the 3d states of gallium.

The first result shows that a one-panel calculation may be sufficient for problems involving only band states around the Fermi level. This will be discussed in the next section with the calculation of the imaginary part of the dielectric function of CoGa in the one-panel and two-panel potentials. On the other hand, when states of lower energies than those of the conduction band are involved, the two-panel calculation must be used. For example, when considering an antisite Al or Ga atom in this series of compounds, Koch and Koenig (1987) have shown that the screening of the defect leads to the formation of either a bound state just below the conduction band or a resonance at the bottom of this band. It is obvious that in the case of CoGa a bad description of the gallium 3d states can have great repercussions on the behaviour of the local densities of the Ga antistructure defect near the bottom of the conduction band. Therefore, to obtain quantitative results, this calculation must be performed with two energy panels.

A comparison of this band structure with x-ray emission spectra would be a good test for the position of the 3d Ga states. Unfortunately, experimental results are only available for Al compounds (Alouani and Khan 1987 and references therein) but not for CoGa.

3. Interband transitions

We present here the calculation of the imaginary part of the dielectric function for these compounds. The numerical method is first tested on the well known dielectric function of Cu.

3.1. Method of calculation—test on Cu

For a cubic material the interband contribution to the imaginary part of the dielectric function at 0 K is given by an integration in the Brillouin zone:

$$\varepsilon_2(\omega) = \frac{e^2}{3\pi m^2 \omega^2} \sum_{nn'} \int \frac{|P_{nn'}(\boldsymbol{k})|^2}{|\nabla \omega_{nn'}(\boldsymbol{k})|} \, \mathrm{d}S$$

where n and n' refer respectively to the occupied and empty states, $P_{nn'} = \langle n'\boldsymbol{k}|P|n\boldsymbol{k}\rangle$ is the dipole matrix element between the initial state $|n\boldsymbol{k}\rangle$ and the final state $|n'\boldsymbol{k}\rangle$ with eigenvalues $E_n(\boldsymbol{k})$ and $E_{n'}(\boldsymbol{k})$, respectively, and $\omega_{nn'}(\boldsymbol{k}) = E_n(\boldsymbol{k}) - E_{n'}(\boldsymbol{k})$ ($\hbar = 1$). The surface S is defined by the $\boldsymbol{k}$-vectors which verify $\omega_{nn'}(\boldsymbol{k}) = \omega$. The eigenfunctions $|n\boldsymbol{k}\rangle$ and the eigenvalues $E_n(\boldsymbol{k})$ are obtained by the LMTO method. Details on the calculation of the dipole matrix elements are given by Koenig and Khan (1983). The reciprocal

space integration is performed by a tetrahedron method, but the integration along surfaces of constant ω are somewhat more complicated than the integration along surfaces of constant energy giving the density of states. The difficulty arises from the cut-off of the Fermi level in a given band n, which is described by a plane $E = E_F$ in each partially contributing tetrahedron. This leads to simple analytical expressions for the density and the number of states (Jepsen and Andersen 1971, Lehman and Taut 1972). On the contrary, for a given interband transition $n \rightarrow n'$, both intersections of bands n and n' with the Fermi level have to be considered. This creates one or two limiting surfaces within a partially contributing tetrahedron, which are neither planes with respect to the variable ω, nor surfaces of constant ω. But the contributing fraction of the volume v_t of the tetrahedron to the transition from n to n' is simple to estimate since it is just the difference between the occupied volumes below E_F in this tetrahedron for the two energy bands n and n'. Rath and Freeman (1975) have shown how to subdivide this fraction of the initial tetrahedron in at most nine microtetrahedra, each of which contributes fully to the transitions. As soon as the values of $\omega_{nn'}$ at their vertices are known, the analytical expressions derived for the densities of states can be used for the integration, by replacing E by ω.

However, it is easy and very fast to proceed numerically instead of analytically inside each partially contributing tetrahedron. The first approximation consists in computing the contribution of this tetrahedron without any cut-off and then weighting the result by the percentage of the volume in which the transitions occur. A further improvement is obtained by a numerical linearisation of the energies and transition probabilities inside each of these tetrahedra subdivided into eight minitetrahedra of equal volume $\frac{1}{8}v_t$. When compared with E_F, this gives again fully contributing, partially contributing and non-contributing minitetrahedra. Then the procedure of weighting is resumed for the partially contributing minitetrahedra. The next step is to subdivide each partially contributing minitetrahedron into eight microtetrahedra of volume $\frac{1}{64}v_t$ before weighting. Figure 3 shows the convergence of this calculation for Cu on an initial grid of 161 $\boldsymbol{k}$ points in the irreducible zone. In this case, the use of microtetrahedra of volume $\frac{1}{64}v_t$ induces an increase of less than 20% computing time compared with the first calculation on the initial grid. A last subdivision of each microtetrahedron into eight ($v_t/512$) does not improve the results. The use of a finer initial mesh of 946 $\boldsymbol{k}$ points or 2856 points modifies slightly the intensities of the peaks but not their positions (figure 4). Figure 4 also compares the results on a grid of 946 points when the f $\rightarrow$ d and d $\rightarrow$ f transitions are added. In that range of energies the f states are mainly hybridisation states. They give a nearly constant contribution which could be neglected when comparing the experiments.

The small downward shift of the calculated dielectric function compared with experimental results (Pells and Shiga 1969, Johnson and Christy 1972) is probably due to the absence of self-energy corrections in our calculation (figure 5). These corrections have been taken account of through a fitting parameter in the work of Janak *et al* (1975). We get the right order for the intensity of the transition without including corrections beyond the atomic sphere approximation (ASA) within the LMTO theory. This is in agreement with the previous result of Alouani *et al* (1986) who found that the ASA gives satisfactory results for the optical properties. However, Uspenski *et al* (1983) have obtained a lower curve for $\varepsilon_2(\omega)$ by a LMTO calculation including these muffin-tin corrections.

This calculation, together with the lifetime broadening effect when comparing the theoretical with the experimental curve, shows that a grid of about 1000 $\boldsymbol{k}$ points gives a good description of the dielectric function. This is then applied to the TAl compounds and CoGa.

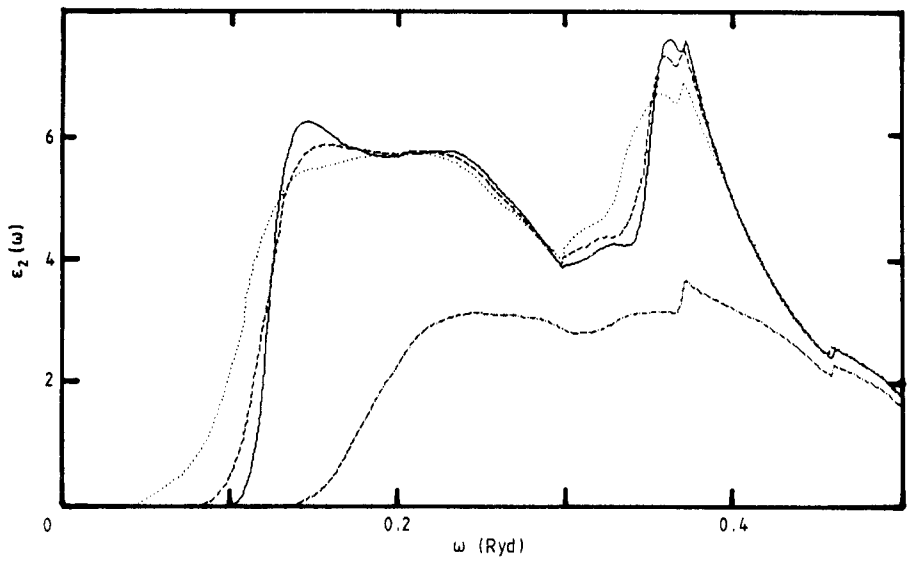

Figure 3. $\varepsilon_2(\omega)$ for Cu, 161 $\boldsymbol{k}$ points: chain curve, partially contributing tetrahedra suppressed; dotted curve, partially contributing tetrahedra weighted; broken curve, partially contributing tetrahedra subdivided into eight minitetrahedra; full curve, partially contributing minitetrahedra subdivided into eight microtetrahedra.

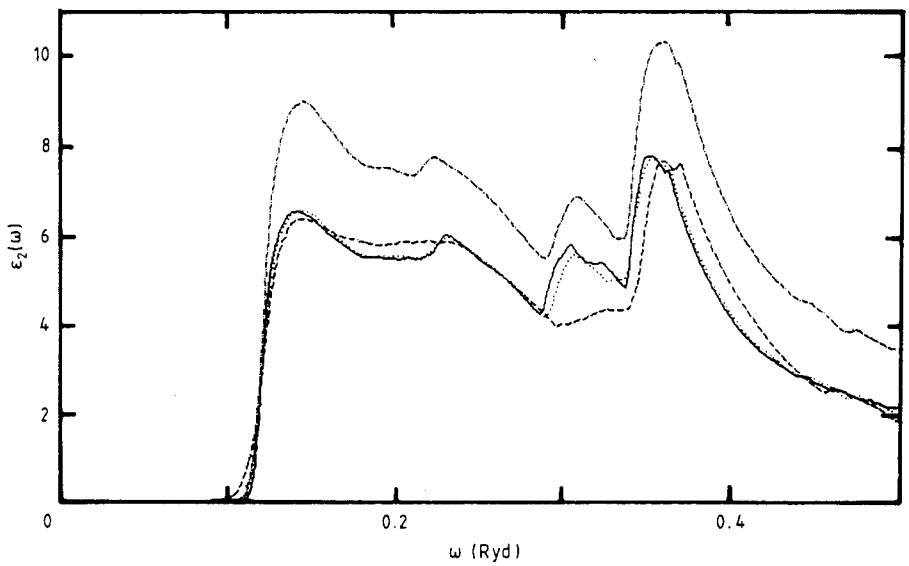

Figure 4. $\varepsilon_2(\omega)$ for Cu: broken curve, 161 points, s, p and d states; broken curve, 946 points, s, p and d states; full curve, 2856 points, s, p and d states; chain curve, 946 points, s, p, d and f states.

3.2. Results

For all these ordered compounds, the matrix elements of P are exactly calculated on a grid of 969 $\boldsymbol{k}$ points in the irreducible wedge of the simple cubic BZ, in order to ensure

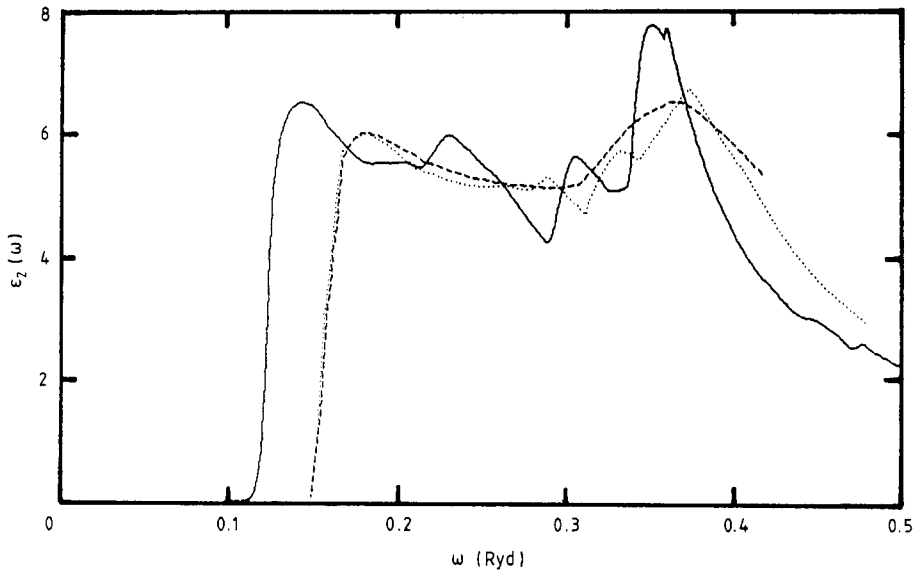

Figure 5. $\varepsilon_2(\omega)$ for Cu: broken curve, experimental curve (Pells and Shiga 1969); dotted curve, calculated curve (Janak *et al* 1975); full curve, our calculated curve for 946 points and with s, p and d states.

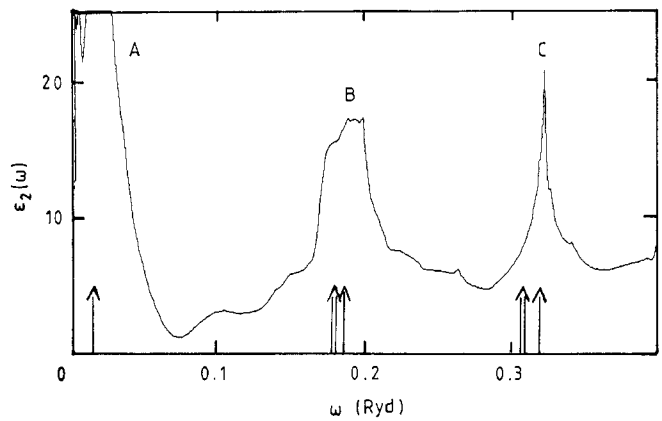

Figure 6. $\varepsilon_2(\omega)$ for NiAl. Single arrow, theoretical position of the peaks, calculated by Eibler and Neckel (1980); double arrow, experimental results (Kiewit and Brittain 1970).

that the integration procedure with $\frac{1}{64}$ fractions of the partially contributing tetrahedra provides convergent results.

(*a*) The $\varepsilon_2(w)$ obtained for NiAl has three peaks (figure 6). Their position is in very good agreement with those calculated by Eibler and Neckel (1980) using a hybridised nearly-free-electron-tight-binding (NFE-TB) interpolation scheme and those obtained experimentally (Kiewit and Brittain 1970, Rechtien *et al* 1967). The first peak cannot be seen experimentally because of Drude's term.

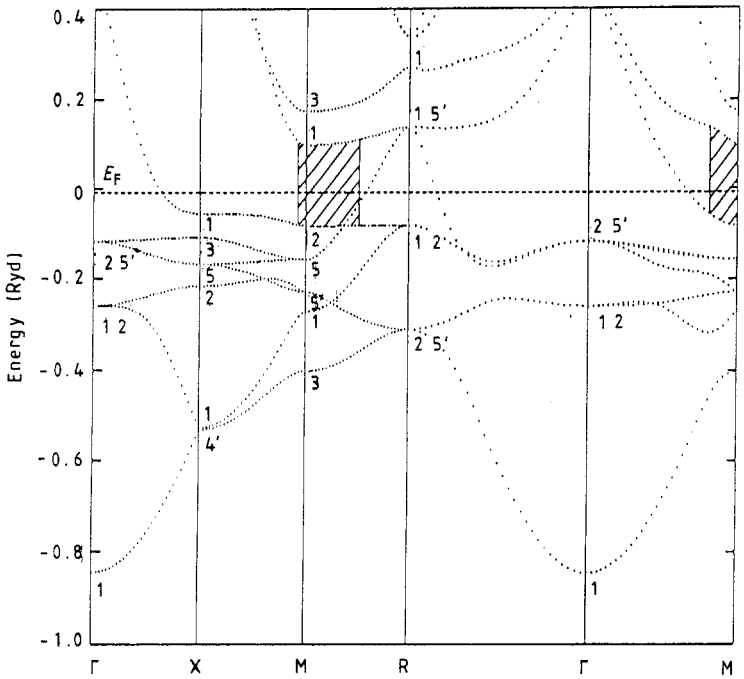

Figure 7. Energy bands in NiAl.

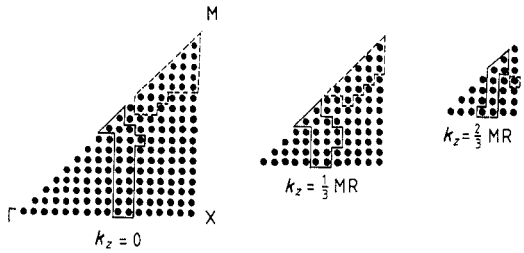

Figure 8. Three sections of the irreducible Brillouin zone of NiAl: $k_z = 0$, $k_z = \frac{1}{3}$MR, $k_z = \frac{2}{3}$MR; broken lines, $\boldsymbol{k}$ points responsible for peak B; full lines, $\boldsymbol{k}$ points responsible for peak C.

A more detailed study shows that peak A of figure 6 is due to transitions from band 6 to band 7 (the bands are numbered in increasing energy order) which occur in the bulk of the BZ of NiAl. Therefore these transitions cannot be seen along high symmetry directions in figure 7. For peak B the more important transitions are from bands 5 and 7 to band 8, and for peak C from band 2 to band 7. In order to localise the $\boldsymbol{k}$ points concerned in these transitions, we represent in figure 8 three sections of the BZ ($k_z = 0$, $k_z = \frac{1}{3}$MR, $k_z = \frac{2}{3}$MR). The $\boldsymbol{k}$ points surrounded with a broken line are responsible for peak B and those surrounded with a full line for peak C. For peak B some transitions occur along the MR, MX and ΓM directions (hatched region in figure 7) whereas the greatest part of the transitions of peak C occur in the bulk of the BZ.

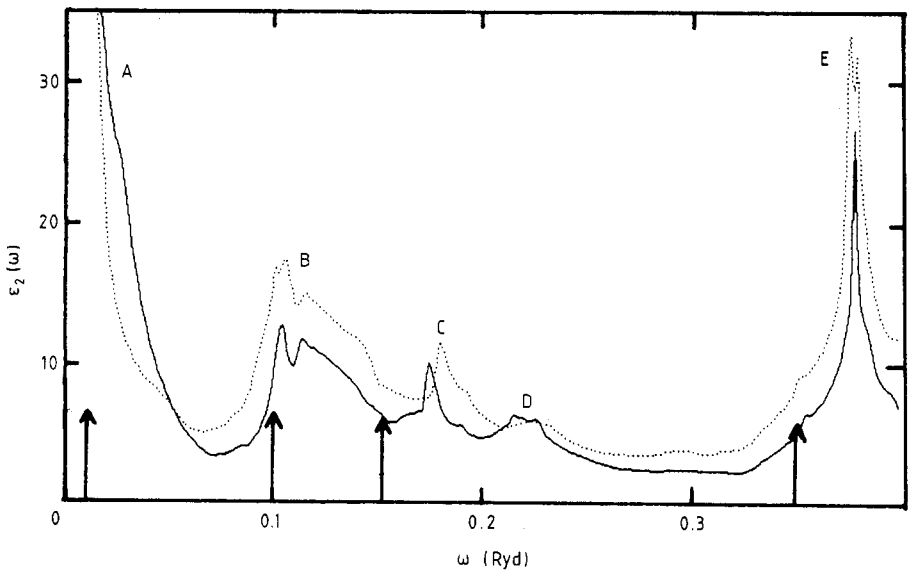

Figure 9. $\varepsilon_2(\omega)$ for FeAl: full curve, s, p and d states; dotted curve s, p, d and f states. Single arrow, theory (Eibler and Neckel 1980).

(*b*) For FeAl (figure 9), the differences with the dielectric function presented in a previous work by Koenig and Khan (1983) (which was given in arbitrary units) are due to the introduction of relativistic effects in the potentials and mainly to the improvement of the reciprocal space integration as described in § 3.1. The introduction of d → f and f → d transitions in the calculation (dotted curve) does not modify the structure of the curve. Figure 9 compares $\varepsilon_2(\omega)$ for FeAl with that of Eibler and Neckel (1980). The D peak does not exist in their curve. Unfortunately no measurements of the imaginary part of the complex dielectric constant are available.

Peaks A and E of FeAl have the same origin as peaks A and C, respectively, of NiAl. Compared with the case of NiAl, the bands 5 and 7 are now above the Fermi level in the region along XM and MR directions, which forbids transitions from these bands to band 8 (responsible for peak B in NiAl). But new transitions are available towards bands 6 and 7. They are responsible for peaks B, C and D of FeAl. We have indicated in figure 10 the different regions where these transitions occur (hatch region for peak B, dotted region for peak C and crosses for peak D).

(*c*) Figure 11 shows $\varepsilon_2(\omega)$ for CoAl. It shows two important peaks which also exist in the results of Eibler and Neckel (1980). Experimentally (Kiewit and Brittain 1970), the first peak is masked by Drude's term; the second is somewhat lower in energy (figure 11).

As for peak A in NiAl and FeAl, peak A in CoAl is mainly due to transitions from band 6 to band 7. But in this compound the number of $\boldsymbol{k}$ points where the transitions occur is more important than in the two preceding compounds because of the position of the Fermi level just below band 7 in the vicinity of point X (hatched region in figure 12). This explains the differences between the form of this peak in CoAl and that observed in NiAl and FeAl. The peak B has the same origin as peak C in NiAl and peak E in FeAl. Figure 12 also shows possible transitions from bands 5 and 7 to 8 along the

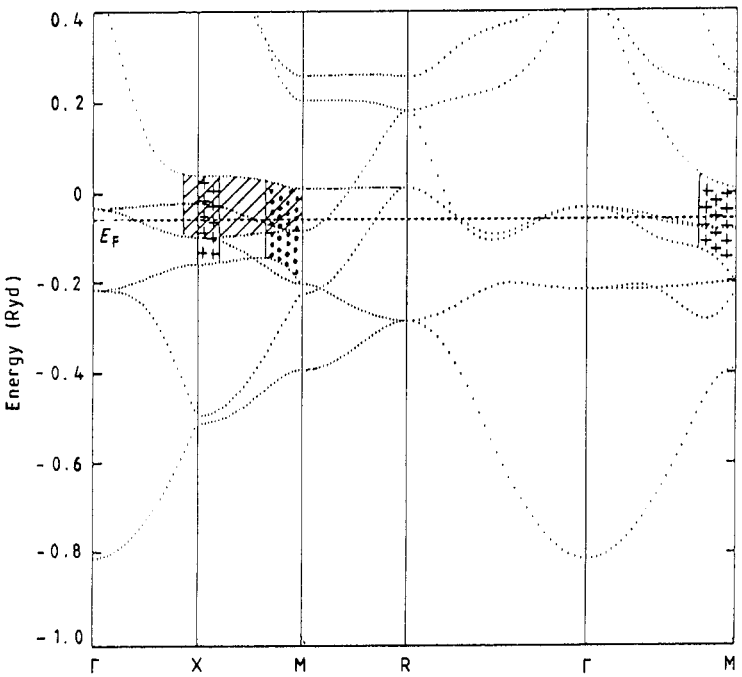

Figure 10. Energy bands in FeAl.

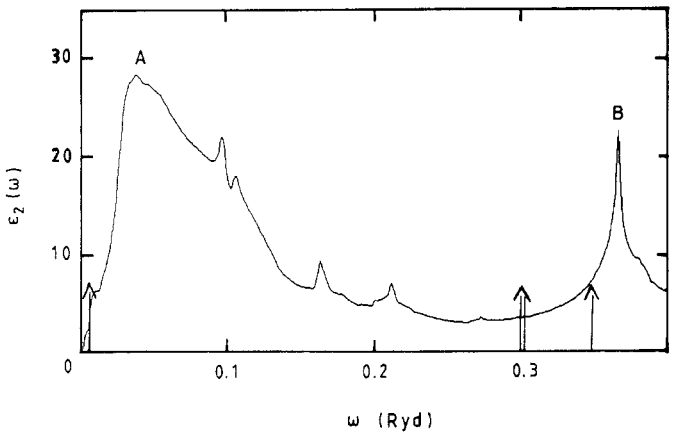

Figure 11. $\varepsilon_2(\omega)$ for CoAl. Single arrow, theory (Eibler and Neckel 1980); double arrow, experimental results (Kiewit and Brittain 1970).

MR direction. But, contrary to NiAl (peak B), there is no corresponding peak in the curve because band 7 rises above the Fermi level outside the MR direction. There are only 42 $\boldsymbol{k}$ points out of 969 below E_F in this band, against 540 in NiAl.

(*d*) CoAl (figure 11) and CoGa (figure 13) show very similar dielectric function curves since the Fermi level has an equivalent position in these two compounds. The origin of the two peaks in CoGa is the same as in CoAl. No other theoretical curves of

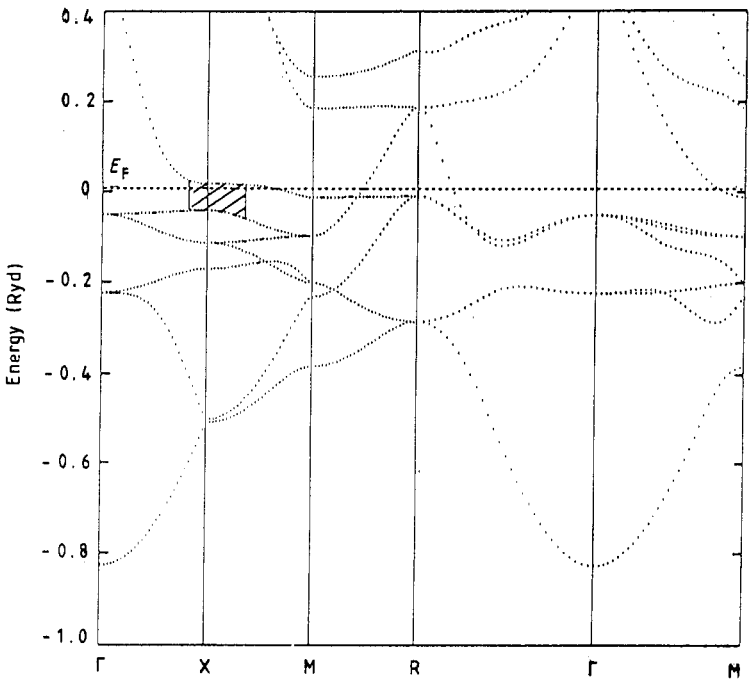

Figure 12. Energy bands in CoAl.

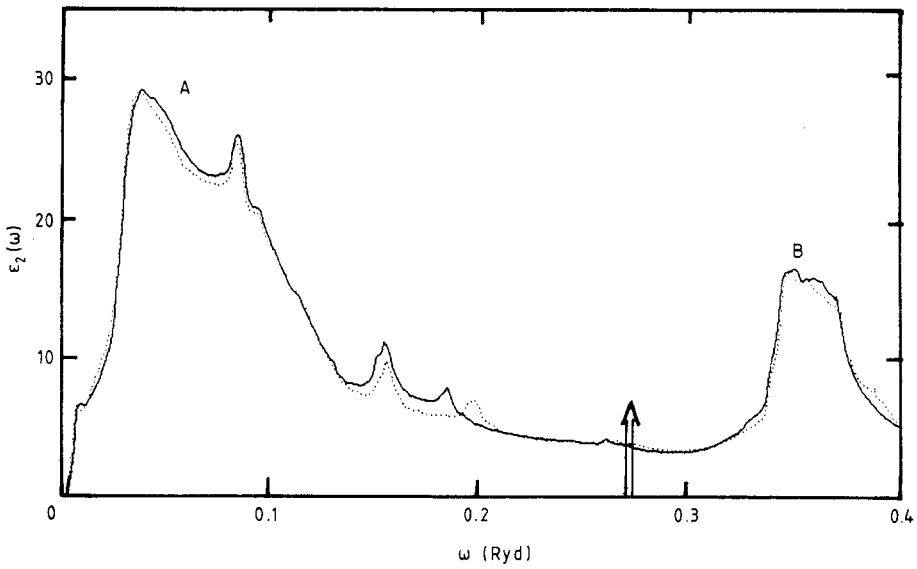

Figure 13. $\varepsilon_2(\omega)$ for CoGa. Double arrow, experimental results (Kiewit and Brittain 1970).

$\varepsilon_2(\omega)$ for CoGa were found for comparison. Experimentally the first peak is masked by Drude's term; the second peak is lower in energy than ours but very small and broad (Kiewit and Brittain (figure 13)).

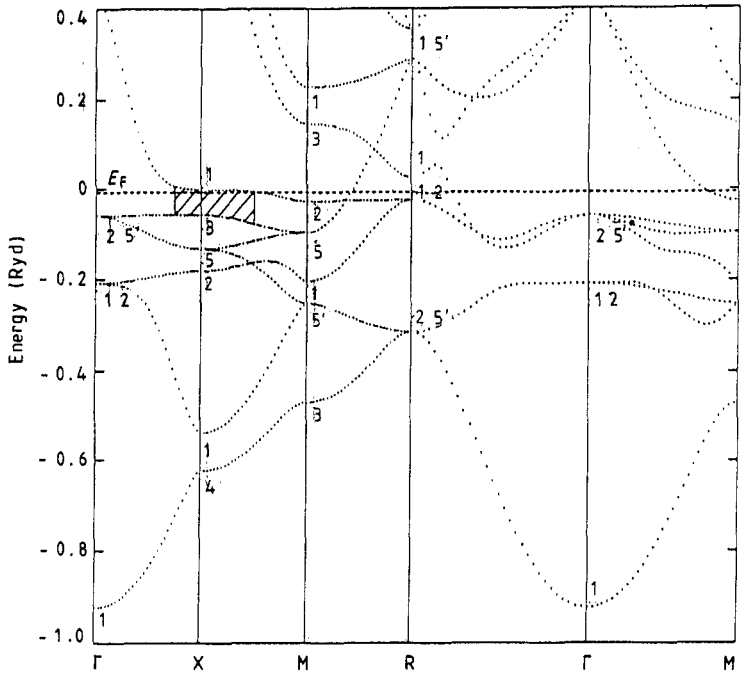

Figure 14. Energy bands in CoGa.

The dotted line in figure 13 represents $\varepsilon_2(\omega)$ obtained for CoGa by a one-panel calculation. The similarity of the two curves shows that a one-panel calculation is sufficient to provide good results for the dielectric function.

4. Conclusion

The density of states of CoGa has been calculated by the LMTO method with 3d states of gallium treated either as core states or included in the self-consistent process. The effect of the delocalisation of the 3d levels on the form of the conduction band density is not very large, but it allows us to correct the unphysical position of the band formed by these states, just below the conduction states. Therefore, to have a good description of the bottom of the conduction band, it is necessary to include the 3d orbitals of gallium in the self-consistent process.

Our optical spectra are in good overall agreement with the previous calculation of $\varepsilon_2(\omega)$ and measured data for the series TAl.

Acknowledgments

The computations were carried out on the IBM 3090 of the CNRS (Centre National de la Recherche Scientifique) in Strasbourg–Cronenbourg, with a grant from the Ministère de l'Education Nationale for the development of intensive numerical calculations. We wish especially to thank B Speckel for the numerical optimisation of the program.

References

Alouani M and Khan M A 1987 *J. Phys. F: Met. Phys.* **17** 519–41
Alouani M, Koch J M and Khan M A 1986 *J. Phys. F: Met. Phys.* **16** 473–82
Christensen N E and Kollar J 1983 *Solid State Commun.* **46** 727–30
Desclaux J P 1975 *Comput. Phys. Commun.* **9** 31
Eibler R and Neckel A 1980 *J. Phys. F: Met. Phys.* **10** 2179–95
Janak J F, Williams A R and Moruzzi V L 1975 *Phys. Rev.* B **11** 1522–36
Jepsen O and Andersen O K 1971 *Solid State Commun.* **9** 1763–7
Johnson P B and Christy R W 1972 *Phys. Rev.* B **6** 4370–9
Kiewit D A and Brittain J O 1970 *J. Appl. Phys.* **41** 710–16
Koch J M and Koenig C 1986 *Phil. Mag.* B **54** 177–97
—— 1987 *Phil. Mag.* B **55** 359–75
Koenig C and Khan M A 1983 *Phys. Rev.* B **27** 6129–35
—— 1988 *Phys. Rev.* B **38** 5887–98
Kubo Y, Wakoh S and Yamashita J 1976 *J. Phys. Soc. Japan* **41** 1556–61
Lehman G and Taut M 1972 *Phys. Status Solidi* b **54** 469–77
Maksimov E G, Mazin I I, Rashkeev S N and Uspenski Y A 1988 *J. Phys. F: Met. Phys.* **18** 833–49
Norman M R and Koelling D D 1985 *Phys. Rev.* B **31** 6251–60
Pells G P and Shiga M 1969 *J. Phys. C: Solid State Phys.* **2** 1835–46
Rath J and Freeman A J 1975 *Phys.Rev.* B **11** 2109–17
Rechtien J J, Kannewurf C R and Brittain J O 1967 *J. Appl. Phys.* **38** 3045–50
Schwartz K, Neckel A and Nordgren J 1979 *J. Phys. F: Met. Phys.* **9** 2509–21
Uspenski Y A, Maksimov E G, Rashkeev S N and Mazin I I 1983 *Z. Phys. B: Condens. Matter* **53** 263–70
Whittle G L, Fletcher G C, Clark P E and Cywinski R 1982 *J. Phys. F: Met. Phys.* **12** 303–16
Zemach R, Ashkenazi J V and Ehrenfreund E 1989 *Phys. Rev.* B **39** 1884–90